Supramolecular Hierarchical Polyurethane Elastomers for Thermal and Mechanical Property Optimization

Ru-Qiang Lu[1,2,+], *Alberto Concellón*,[1,2,+] *Pan Wang*,[1,2,+] *Timothy M. Swager*[1,2,*], *Alex J. Hsieh*[1,*]

[1]Institute for Soldier Nanotechnologies, MIT, Cambridge, Massachusetts 02139, USA; [2]Department of Chemistry, MIT, Cambridge, Massachusetts 02139, USA

ABSTRACT

Supramolecular chemical designs that integrate complementary hydrogen bond donor and acceptor complexes in hierarchical polyurethane elastomers are reported. N^2,N^6-bis(2-hydroxyethyl)pyridine-2,6-dicarboxamide (PDA) and 5,5-bis(3-hydroxypropyl)barbituric acid (BBA) react with 4,4′-methylenediphenyl diisocyanate (MDI) to produce hard segments capable of multiple intermolecular hydrogen bonds in MDI-PDA/BBA-poly(tetramethylene oxide) (PTMO) polyurethanes. The addition of PDA facilitates the formation of a supramolecular complex, and BBA affords greater intersegmental mixing. As a result, these polyurethanes exhibit higher glass transition temperatures (T_g) and greater strain hardening/strengthening under tensile deformation than a microphase-separated MDI-butanediol (BDO)-PTMO analog. Additionally, increased PDA and BBA contents results in up to a 60 °C increase of T_g determined at 1 Hz via DMA relative to those determined by calorimetric measurements via DSC, which is considerably higher than the 15 °C T_g increase observed in the MDI-BDO-PTMO analog. These results highlight a significant interplay between intersegmental mixing and supramolecular hydrogen bond interactions for the design of robust hierarchical elastomers.

Corresponding Authors: *Timothy M. Swager, tswager@mit.edu; *Alex J. Hsieh, ajhsieh@mit.edu.

KEYWORDS: Hierarchical polyurethane elastomers; supramolecular hydrogen bond interactions; intersegmental mixing; dynamic glass transition temperatures; mechanical properties.

1. Introduction

Thermoplastic polyurethanes are highly versatile elastomers that contain soft and hard segments. The flexible segments impart elasticity at room temperature, whereas the self-assembly of rigid segments leads to the formation of a physically cross-linked network. The microstructure in these materials strongly influences the composition-dependent thermal, physical and mechanical properties.[1-11] The ability to combine chemically dissimilar structures has led to the use of these hierarchical elastomers in a broad range of applications including thin film adhesives,[12] elastic fibers for textiles,[13] synthetic rubbers and foams[14], bio-compatible membranes, medical components,[15-17] as well as binder resins for prepreg-based fiber composites.[18] There have been extensive studies with respect to the complex interplay between hard and soft segment thermodynamic compatibility and the extent of intermolecular hydrogen bonding interactions.[9-11] High symmetry diisocyanates, such as aromatic 1,4′-phenylene diisocyanate or aliphatic hexamethylene diisocyanate (HDI), give rise to strong intermolecular monodentate hydrogen bond interactions between the hard segments, and promote microphase separation.[9-11] Additionally, the realization of a novel high-rate deformation-induced rubber-to-glass transition mechanism has inspired significant interest in polyurea,[19-24] poly(urethane urea),[25-33] and polyurethane-based elastomeric materials.[34-38] In these classes of elastomers, it was reported when the segmental relaxation times are similar to the strain rates during impact, and a viscoelastic rubber-to-glass transition provides for a large energy absorption and dissipation capability.[19, 20] Furthermore, new insight derived from Hugoniostat simulations suggests that the material deformation under shock loading is dominated by the soft domain response.[38] This conclusion was rationalized through a comparison between a segmented polyurethane and polyethylene.[38]

A recent study focused on two-component polyurethanes based on the stoichiometric reactions of poly(tetramethylene oxide) (PTMO, M_n = 650 g/mol) with either aliphatic HDI or aromatic 4,4′-methylenediphenyl diisocyanate (MDI), but lacking a chain extender.[36] This pseudo soft-phase composition, allowed for the clear elucidation of the molecular structure influence on the extent of intersegmental hydrogen bond interactions, as well as their influence on segmental dynamics and the dynamic glass transition temperature (T_g) of PTMO.[36] Additionally, high strain-rate microparticle impact deformation measurements revealed that a predominantly-amorphous MDI-

PTMO 650 polyurethane exhibits greater dynamic stiffening than the semicrystalline HDI-PTMO 650.[36] This occurs despite the symmetry of HDI producing higher-order monodentate carbamate moieties and a higher ambient storage modulus.[36] Adding butanediol (BDO) to form segmented MDI-BDO-PTMO 650 polyurethane, as expected, results in higher dynamic stiffening and strengthening characteristics when compared to MDI-PTMO 650.[37] In comparison, polyurea and poly(urethane urea) elastomers, both comprising bidentate hydrogen bond interactions, revealed higher threshold velocity values for penetration of impacting microparticles than MDI-BDO-PTMO 650.[37]

Molecule design efforts continue to explore new syntheses for hierarchical polyurethane-based materials with novel and multi-functionalities.[39-43] Ion-containing segmented polyurethane copolymers have demonstrated that charged groups (both cationic and anionic) have a strong influence on the polymer microstructure, through disruption of hydrogen bonding and aggregation of ionic groups.[40] Incorporating diol-functionalized trisaminocyclopropenium (TACP) carbocations as chain extenders in HDI-PTMO based polyurethanes, Lambeth and coworkers reported that the presence of TACPs caused different crystallization behavior of PTMO when compared to the HDI-BDO-PTMO control.[40] In the latter case, the regioregular structure of the HDI-BDO hard segment presumably led to formation of strong hydrogen bonding interactions and hard segment crystalline domains.[40]

In this work, we investigate an alternative supramolecular chemistry approach through incorporation of N^2,N^6-bis(2-hydroxyethyl)pyridine-2,6-dicarboxamide (PDA) and 5,5-bis(3-hydroxypropyl)barbituric acid (BBA) for reaction with MDI to form hard-segment domains. In these polyurethanes the complementary PDA and BBA monomers bind together and/or interact separately in the soft phase producing multiple intermolecular hydrogen bonds. Our investigations access the supramolecular complex formation, and potential synergistic effects of PDA and BBA for the formation of higher cohesive energy density, tailoring of microstructure-mediated dynamic T_g of PTMO, and overall mechanical property optimization. The extent of hydrogen bonding was determined by attenuated total reflectance-Fourier transform infrared spectroscopy (ATR-FTIR). Additionally, the composition influence on microstructure, glass transition temperature measured by differential scanning calorimetry (DSC) and dynamic mechanical analysis (DMA), as well as on tensile deformation measurements will be discussed.

2. Experimental

2.1 Materials

All chemicals were used as received if they are not otherwise noted. Monomers PDA[44] and BBA[45] were synthesized according to reported procedures. MDI-BDO-650 was synthesized in our previous report.[37]

2.2 Synthesis

General procedure. The synthesis of random polyurethanes followed the reported procedures with modifications.[36, 46, 47] Specifically, PTMO (M_n = 650 g/mol) was dried under vacuum for 1-2 h at 50 °C. PDA, BBA and anhydrous DMF were added under Ar, and the mixture was sonicated until all solids dissolved. Subsequently, 4,4′-methylenediphenyl diisocyanate (MDI) (-OH/-NCO molar ratio is ~1/1.1) and dibutyltin dilaurate (DBTDL, 3 drops) were added under Ar. The reaction mixture was stirred at room temperature for 48 h, followed by the addition of anhydrous methanol (3 mL). The mixture was further stirred for 1h, thereafter, the solution was precipitated in methanol, and the solid was collected by centrifuge. The solid was re-dissolved in tetrahydrofuran (THF), filtered by a syringe filter (pore size: 1 μm) and re-precipitated two times using hexane and methanol, respectively. The final solid was dried at 80 °C under vacuum for 24 h. The synthesis of the PDA- and/or BBA-modified polyurethanes is illustrated in Figure 1. In the sample nomenclature, the numerals in PDAxBBAy refer to the respective molar content of PDA and BBA in a stoichiometric ratio of MDI:PDA:BBA:PTMO, where [MDI] = [PDA] + [BBA] + [PTMO]. Table 1 lists the compositions including the wt.% of each component in PDA/BBA-polyurethanes, and hard segment only HS_PDABBA-polyurethanes. For MDI-BDO-650 with a stoichiometric ratio 2:1:1, the wt.% of MDI, BDO, and PTMO is 40.9%, 7.2%, and 51.9%, respectively.

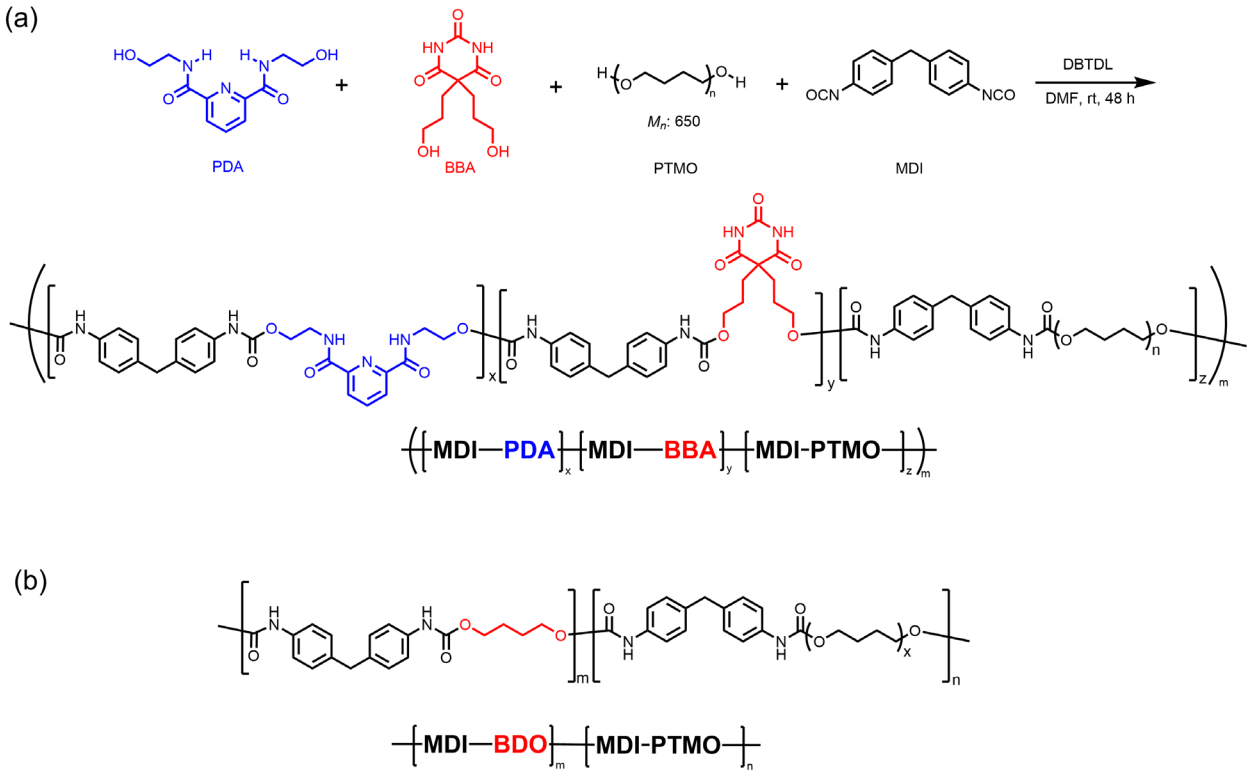

Figure 1. (a) Synthesis of PDA and/or BBA-containing polyurethanes. (b) Chemical structure of MDI-BDO-650.

Table 1. Compositions of PDA/BBA-polyurethanes, and hard segment only HS_PDABBA-polyurethanes.

	MDI:PDA:BBA:PTMO	Wt.%			
		MDI	PDA	BBA	PTMO
PDA0BBA0	100:0:0:100	29.7	0	0	70.3
PDA26BBA0	126:26:0:100	32.6	6.1	0	61.3
PDA0BBA26	126:0:26:100	32.7	0	5.9	61.4
PDA100BBA0	200:100:0:100	37.9	17.4	0	44.7
PDA0BBA100	200:0:100:100	38.1	0	16.9	45.0
PDA13BBA13	126:13:13:100	32.6	3.1	3.0	61.3
PDA37BBA37	174:37:37:100	36.5	7.1	6.9	49.5

PDA50BBA50	200:50:50:100	38.0	8.7	8.4	44.9
PDA60BBA60	220:60:60:100	39.0	9.8	9.4	41.8
HS_PDA100	100:100:0:0	52.2	47.8	0	0
HS_BBA100	100:0:100:0	53.0	0	47.0	0
HS_PDA100BBA100	200:100:100:0	52.6	24.1	23.3	0

2.3 Characterization

Gel permeation chromatography (GPC) measurements of molecular weights were performed in THF using an Agilent 1260 Infinity system and calibrated with polystyrene standards. Attenuated total reflectance – Fourier transform infrared (ATR – FTIR) spectra were acquired using a Thermo Scientific Nicolet 6700 Fourier transform infrared spectrometer. NMR spectra were collected on a Bruker Avance 400 MHz or 500 MHz spectrometer. Chemical shifts are reported in ppm and referenced to residual NMR solvent peaks (^{1}H NMR: THF-d_8: δ 1.73 and 3.58 ppm, DMSO-d_6: δ 2.50 ppm).

Small-angle X-ray scattering (SAXS) measurements were performed with a SAXSLAB instrument equipped with a Rigaku 002 microfocus X-ray source ($CuK_{\alpha 1}$ = 1.5409 Å) and a Dectris Pilatus 300K detector that moves from 100 mm to 1500 mm from the sample. The sample-to-detector distance was 459.1 mm, and the beam center and the q range were calibrated using the diffraction peaks of silver behenate.

Thermal properties were determined by differential scanning calorimetry (DSC) using a TA Instruments Discovery DSC instrument. Two heating-cooling cycles were performed from −90 to 180 °C at a scan rate of 10 °C/min using sealed aluminum pans under N_2 atmosphere. Glass transition temperatures (T_g) were determined at the half‐height of the baseline jump from the second heating scan. Dynamic mechanical analysis (DMA) was performed on a TA Instruments Q850 instrument at 1 Hz with a strain of constant amplitude of 20 μm from −120 to 120 or 140 °C. The heating rate for DMA is 3 °C/min.

Tensile tests were performed on an 8848 MicroTester (Instron) (extension rate: 0.1 mm/s, load cell: 50 N). The dog-bone specimens with a gauge length of 10 mm and a gauge width of 1.65 mm were cut out using a ASTM-D412-C 0.25 scale die cutter.[48] Details on specimens preparation

for tensile measurements as well as for other materials characterization can be found in the Supplementary Information section.

3. Results

3.1 Bottom-up design by incorporation of PDA and BBA

To understand the influence of molecular structures, we investigated a series of compositions with varying amounts of PDA and BBA in their structure, PDAxBBAy, where x = 0, 26, and 100, and y = 0, 26, and 100 (see Table 1 for the labeling details). Figures 2a and 2b compare the ATR-FTIR spectra obtained for polyurethanes having PDA and BBA, but not both (PDA0BBA0, PDA26BBA0, PDA100BBA0, PDA0BBA26, and PDA0BBA100). The baseline polyurethane, PDA0BBA0, displays the well-defined stretching modes for free and hydrogen bonded carbonyls at approximately 1728 cm^{-1} and 1704 cm^{-1}, respectively, and the hydrogen bonding amide protons at 3297 cm^{-1}. Figures 2c and 2d show the carbonyl and amide hydrogen stretching bands for the bulk "hard-segment" only of the three different systems HS_PDA100, HS_BBA100, and HS_PDA100BBA100, as well as for PDA and BBA monomers.

Polymers with PDA display a carbonyl stretching band at approximately 1665-1667 cm^{-1} for both PDA26BBA0 and PDA100BBA0, which has an intensity that increases with PDA content (Figure 2b). This band is not observed in PDA0BBA0, PDA0BBA26, and PDA0BBA100, which is at higher energy than that of the PDA monomer at 1656 cm^{-1}, and is more intense in HS_PDA100 when compared to HS_PDA100BBA100 (Figure 2d). For the latter, the intensity variation could also be affected by BBA conformation restrictions, which prevents intermolecular hydrogen bond interactions between the neighboring carbamate moieties in the hard-segment-only HS_PDA100BBA100. It is noteworthy that in Figure 2b, the relative intensity ratio of PDA0BBA100's carbamate hydrogen bonded/non-bonded carbonyl stretching bands (1700 cm^{-1} and 1725 cm^{-1}, respectively) is significantly higher than the carbamate bands observed for PDA0BBA0. Additionally, there is a shift in the carbonyl stretching from 1700 cm^{-1} for the BBA monomer to 1693 cm^{-1} for the hard segment HS_BBA100, as shown in Figure 2d. These results are strongly indicative of an affinity, or intersegment mixing, between BBA and carbamate

moieties. In comparison, HS_PDA100 (Figure 2d) displays a moderate intensity carbonyl stretching band at 1665 cm^{-1}, suggesting higher ordering in hard segment composition.

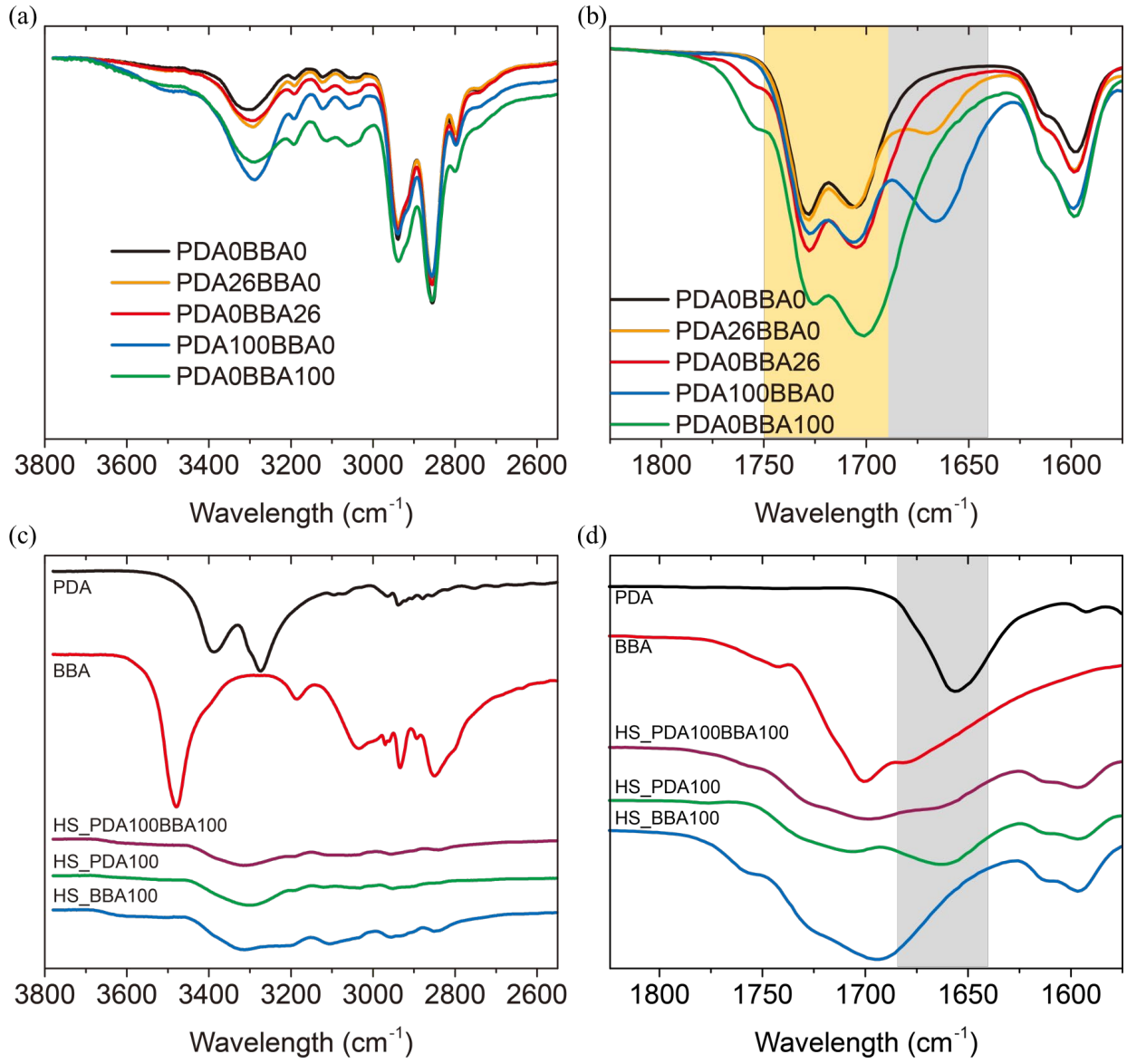

Figure 2. ATR-FTIR spectra in the (a) N–H and (b) carbonyl stretching regions for PDA0BBA0 (black), PDA26BBA0 (orange), PDA0BBA26 (red), PDA100BBA0 (blue), and PDA0BBA100 (green). ATR-FTIR spectra in the (c) N–H and (d) carbonyl stretching regions for PDA (black), BBA (red), HS_PDA100BBA100 (purple), HS_PDA100 (green), and HS_BBA100 (blue). In (b)

and (d), the shaded regions correspond to the carbonyl stretching bands associated with PDA (grey) and carbamates (orange), respectively.

Figure 3a details SAXS characterization for the hard-segment-containing PDA26BBA0, PDA100BBA0, PDA0BBA26, and PDA0BBA100 polyurethanes, and for a baseline PDA0BBA0 without hard segments. PDA100BBA0 exhibits a modest scattering peak, whereas a broad scattering profile is observed in each of the other three PDA/BBA-containing polyurethanes. Addition of PDA shifts the interference peak to a smaller scattering vector q value, corresponding to an interdomain spacing of 10.2 nm, and greater phase segregation in PDA100BBA0 than in PDA0BBA100. The presence of significantly lower scattering contrast in PDA0BBA100 suggests greater intersegmental mixing in the BBA-containing polyurethane. More details on molecular pathways toward intersegmental mixing facilitated by BBA versus the propensity toward phase contrast with addition of PDA are discussed in Section 3.3.

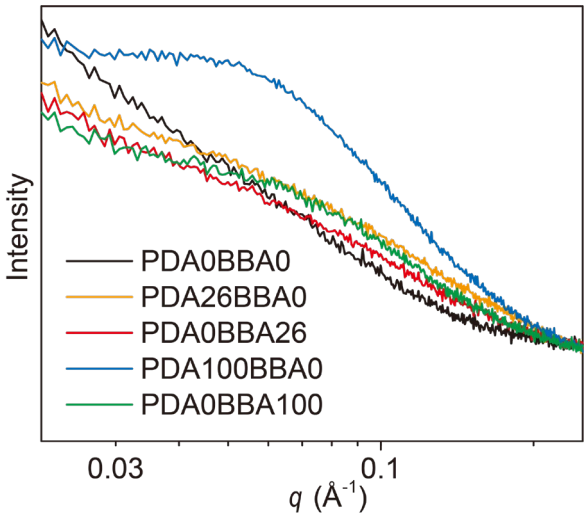

Figure 3. SAXS data showing microstructure changes resulting from the addition of PDA and BBA in PDA26BBA0 (orange), PDA0BBA26 (red), PDA100BBA0 (blue), and PDA0BBA100 (green) compared to the baseline polyurethane PDA0BBA0 (black).

3.2 Influence of chain extenders: PDA and BBA vs. BDO

As an initial step in the material properties characterization, we determined the efficacy of PDA and BBA by comparing PDA100BBA0 and PDA0BBA100 with MDI-BDO-650, where all three

polyurethanes encompass the same stoichiometric ratio of 2:1:1 ([MDI]:[PDA]:[PTMO] in PDA100BBA0, [MDI]:[BBA]:[PTMO] in PDA0BBA100, and [MDI]:[BDO]:[PTMO] in MDI-BDO-650), and correspondingly each has the same molar content of carbamate moieties. In Figure 4a, DSC results indicate that addition of PDA and BBA to form hard segments results in higher T_g values than the baseline material, PDA0BBA0 (-31.1 °C). PDA0BBA100 exhibits slightly higher T_g values than PDA100BBA0, 14.6 °C vs. 7.0 °C, respectively. Higher T_g values are also determined for PDA/BBA-containing polyurethanes than that of PDA0BBA0 using DMA tanδ data measured at 1 Hz, as shown in Figure 4b. Additionally, for PDA100BBA0 and PDA0BBA100 in comparison to PDA0BBA0, the glass transition observed in DSC (Figure 4a) occurs over a broader range as is consistent with a broader tanδ relaxation data, along with a reduction in the relaxation intensity, measured at 1 Hz in DMA (Figure 4b). As revealed in Figure 4a, the DSC T_g values of PDA100BBA0 and PDA0BBA100 are higher than that of MDI-BDO-650, -17.2 ºC. However, the difference becomes more significant in the DMA tanδ data measured at 1 Hz, 67.6 ºC and 61.5 ºC vs. -2.1 ºC, respectively (Figure 4b). MDI-BDO-650 exhibits a melting endotherm (Figure 4a), which is in accord with a well-defined interference peak in SAXS (Figure 4c), and other previously observed in polyurethanes with microphase-separated morphologies.[3, 9, 40] This contrasts with the presence of relatively weak scattering intensity observed in all the polyurethanes containing PDA and BBA (Figure 3), except that PDA100BBA0 exhibits a modest scattering contrast. Table 2 lists the T_g values obtained from both DSC and DMA measurements for these four polyurethanes.

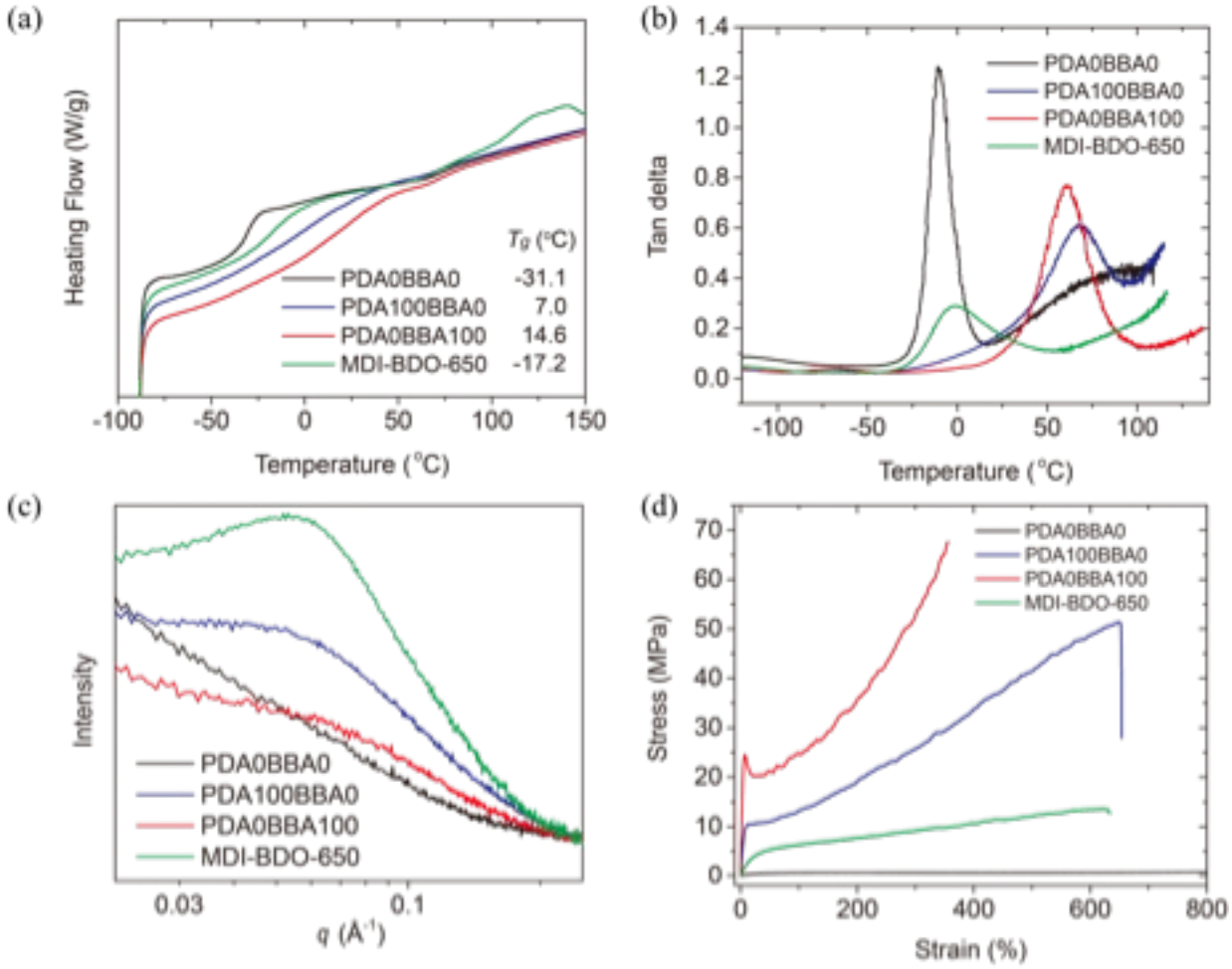

Figure 4. Influence of chain extenders PDA and BBA vs. BDO on thermal, thermomechanical, microstructure, and tensile properties determined by (a) DSC and (b) DMA tanδ at 1 Hz, (c) SAXS, and (d) tensile deformation measurements for PDA0BBA0 (black), PDA100BBA0 (blue), PDA0BBA100 (red), and MDI-BDO-650 (green), respectively.

Table 2. Values of T_g determined from DSC and DMA at 1 Hz, as well as values of ambient storage modulus data from DMA for the baseline PDA0BBA0, PDA100BBA0, PDA0BBA100, and MDI-BDO-650.

	MDI:PDA:BBA:PTMO[a]	M_n (kDa)[b]	PDI	T_g^{DSC} (°C)	T_g^{DMA} (°C)	Storage Modulus (MPa)[c]
PDA0BBA0	100:0:0:100	56.5	2.02	-31.1[d]	-11.0[d]	3.2[d]

PDA100BBA0	200:100:0:100	31.6	1.98	7.0	67.6	539.4
PDA0BBA100	200:0:100:100	104.5	2.62	14.6	61.5	1238.4
MDI-BDO-650	-	-	-	-17.2	-2.1	54.3

[a] Molar ratio. [b] Determined in THF via GPC. [c] Storage modulus at 25ºC. [d] The values obtained for PDA0BBA0 are consistent with those reported previously.[36]

Figure 4d compares the stress vs. strain data obtained from tensile deformation measurements at room temperature for PDA0BBA0, PDA100BBA0, PDA0BBA100, and MDI-BDO-650. PDA and BBA produce hard segments with higher stiffness and higher flow stress values relative to the baseline material, PDA0BBA0. Additionally, PDA0BBA100 reveals a characteristic yield-like behavior with a peak stress determined at 23.9 MPa, and a high T_g (Table 2). PDA0BBA100 also exhibits higher post-yield stress and higher tensile strength values than PDA100BBA0 that has a higher strain at failure and higher toughness. The latter was calculated based on the tensile stress vs. strain data. Both PDA100BBA0 and PDA0BBA100 exhibit significantly higher flow stress values and higher tensile strengths than those of MDI-BDO-650. Table 3 lists the values of flow stress measured at 50% and 200% strain for PDA100BBA0, PDA0BBA100, the baseline PDA0BBA0, and MDI-BDO-650, as well as tensile strength, strain at failure and toughness values for these PDA/BBA-polyurethanes, along with yield stress measured for PDA0BBA100.

Table 3. Values of flow stress measured at 50% strain and 200% strain, as well as tensile strength, strain at failure, yield stress, and toughness for PDA/BBA-polyurethanes and MDI-BDO-650.

	Flow stress (MPa)[a]		Tensile Strength (MPa)[a]	Strain at Failure (%)[a]	Yield Stress (MPa)[a]	Tensile Toughness (MJ/m^3)[a]
	at 50% strain	at 200% strain				
PDA0BBA0	0.49[b]	0.63[b]	-	-	-	-
PDA100BBA0	11.84±0.72	20.16±0.97	55.97±10.42	651±84	-	200±54
PDA0BBA100	20.54±0.58	34.76±0.70	65.48±7.55	348±34	23.92±0.64	122±21

MDI-BDO-650	5.24±0.12	7.53±0.19	13.80±0.46	635±20	-	59±1

[a,b] Tensile properties were calculated based on (a) the average of three measurements ± standard deviation, and (b) an average of two measurements.

3.3 Plausible hydrogen bonding interactions associated with PDA and BBA

To better understand the molecular attributes that enhance the thermal and mechanical properties in PDA100BBA0 and PDA0BBA100 over MDI-BDO-650, we compare the hydrogen bonding interactions associated with PDA and BBA moieties. We hypothesize that incorporation of PDA results in bidentate hydrogen bonding interactions between its carboxamide protons and carbonyls of carbamates.[49] These interactions can either be in the hard segment of PDA-MDI, next to PTMO in the soft phase, as illustrated in Figure 5a, or potentially with the carbonyls of BBA (Figure 5c). It is envisioned that dual hydrogen bonds between BBA and both carbonyl and amide hydrogen moieties of a carbamate are feasible (Figure 5b). Both supramolecular bidentate hydrogen bonds and dual hydrogen bonds formation can occur through either intramolecular or intermolecular interactions. We reason that dual hydrogen bonding interactions are more likely between BBA and carbamate moieties associated with PTMO in the soft phase than the carbamate moieties within the PDA-MDI and BBA-MDI hard segments. The latter would result in greater scattering contrast between hard and soft phases. In support of this assertion, the SAXS data (Figures 3 and 4c) for PDA0BBA100 exhibits an interference peak with significantly less scattering contrast than that of PDA100BBA0. We rationalize that the propensity toward dual hydrogen bonds interactions with carbamates in the soft phase leads to greater intersegmental mixing in PDA0BBA100, along with a higher cohesive energy density than is possible with the monodentate hydrogen bonds association between the carbamate groups in PDA0BBA0 as well as in MDI-BDO-650. This is consistent with PDA0BBA100's high T_g (Table 2) and characteristic yield-like behavior with a peak stress of 23.9 MPa (Figure 4d and Table 3) under tensile deformation.

The conformation preferences associated with the dual hydrogen bond interactions between BBA and carbamate moieties, which are shown in Figure 5b may be an over simplification. We only show cis-amide conformations as they promote multipoint interactions, but there are clearly

trans-amides present in the materials. A more complete analysis of the conformational preferences is beyond the scope of this work.

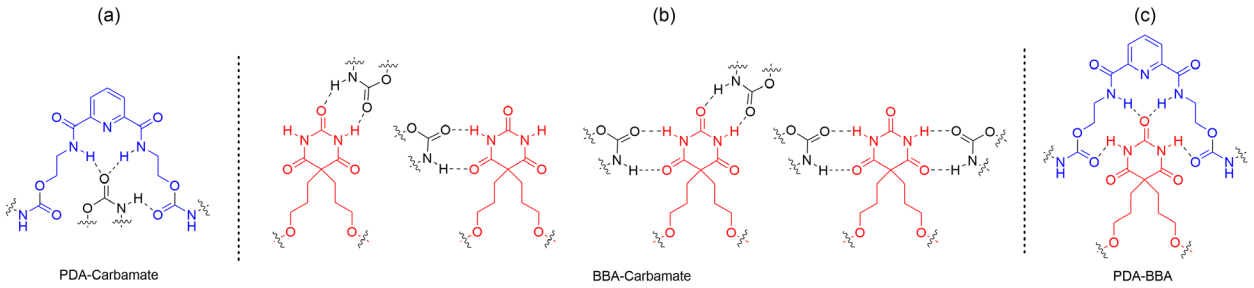

Figure 5. Examples of plausible intramolecular and intermolecular hydrogen bond interactions (a) between PDA and carbamate moieties, (b) between BBA and carbamates, as well as (c) between PDA and BBA in PDA/BBA-polyurethanes.

3.4 Synergy of PDA and BBA for property optimization

Building on our initial results, we designed a second series of polyurethanes containing both PDA and BBA to further investigate the influence of molecular attributes on microstructure, dynamic T_g, and the corresponding mechanical properties. Figure 6 shows the stretching bands of amide hydrogens and carbonyls obtained from ATR-FTIR for PDA13BBA13, PDA37BBA37, PDA50BBA50, and PDA60BBA60. The intensity ratio associated with carbamate hydrogen bonded/non-bonded carbonyl stretching bands (1700 cm^{-1} and 1725 cm^{-1}, respectively) increases with increased hard segment content, but is not as significant as that observed for PDA0BBA100 (Figure 2b). Additionally, the carbonyl stretching band at 1665-1667 cm^{-1} (Figure 6b) is consistent with those previously observed in PDA-containing PDA26BBA0 and PDA100BBA0 (Figure 2b), wherein the peak increases with hard segment content. These observations are consistent with the SAXS scattering contrast in Figure 7, wherein increased PDA/BBA hard segment contents results in the appearance of an interference peak for PDA37BBA37, PDA50BBA50, and PDA60BBA60. PDA50BBA50 and PDA60BBA60 exhibit the highest scattering contrast, but both are lower than that of PDA100BBA0 (Figure 3). These microstructure results strongly suggest an interplay between the presence of a supramolecular PDA/BBA complex which is facilitated by PDA and intersegmental mixing afforded by BBA with the soft phase. For the hard segment HS_PDA100BBA100, the scattering profile shows a broad interference peak at a much lower q

value, which could be the result of interconnected, or significantly disordered, PDA100 and BBA100 hard segments.

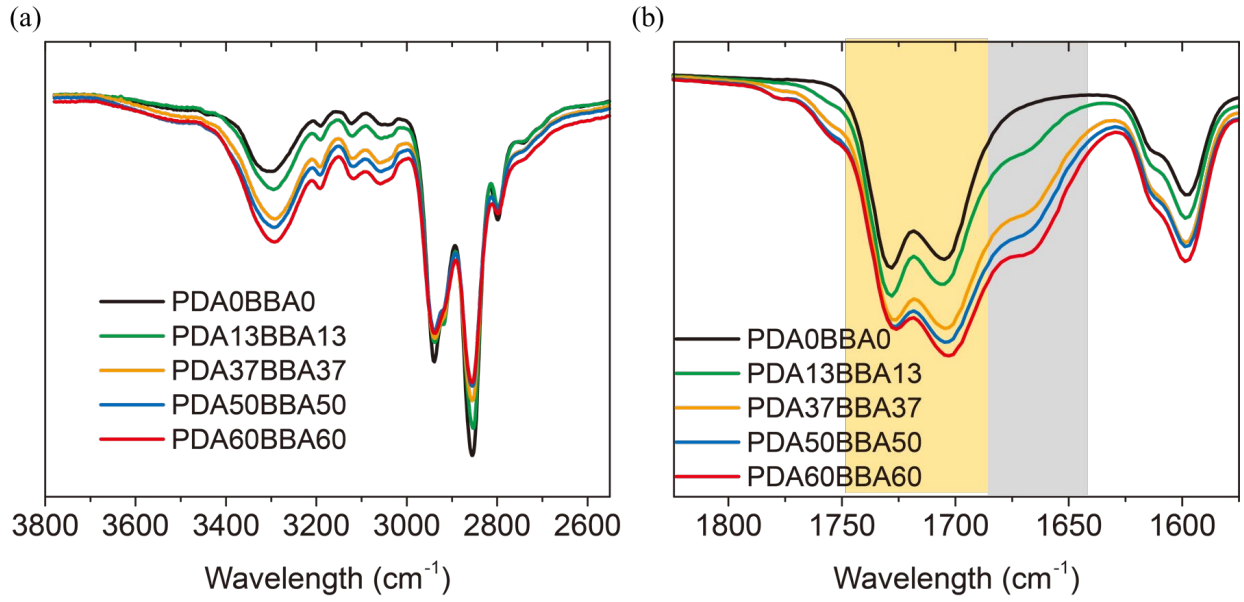

Figure 6. ATR-FTIR spectra in the (a) N–H and (b) carbonyl stretching regions for PDA0BBA0 (black), PDA13BBA13 (green), PDA37BBA37 (orange), PDA50BBA50 (blue), and PDA60BBA60 (red). In (b), the shaded regions correspond to the carbonyl stretching bands associated with PDA (grey) and carbamates (orange), respectively.

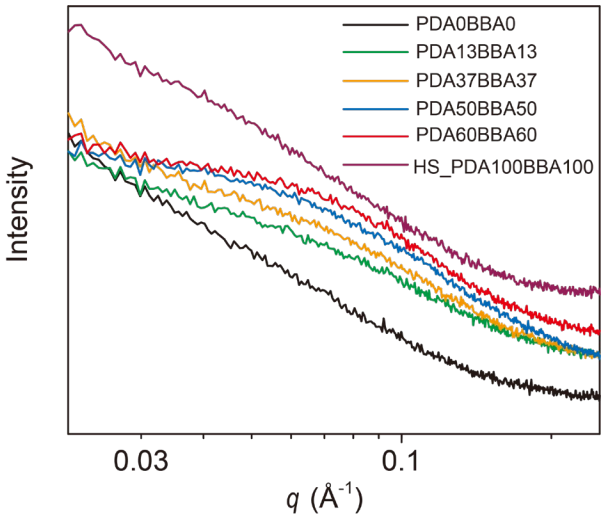

Figure 7. SAXS data for PDA0BBA0 (black), PDA13BBA13 (green), PDA37BBA37 (orange), PDA50BBA50 (blue), PDA60BBA60 (red), and hard segment HS_PDA100BBA100 (purple).

As the PDA/BBA hard segment content increases, T_g of PTMO (the soft phase) increases in PDA/BBA-modified polyurethanes as clearly illustrated in DSC (Figure 8) and DMA (Figure 9) measurements. The DSC thermogram of PDA60BBA60 displays a 45.8 ºC increase in T_g over the baseline PDA0BBA0 (14.7 ºC vs. -31.1 ºC, respectively), and the glass transition is significantly broadened for PDA37BBA37, PDA50BBA50, and PDA60BBA60. Increases in the PDA/BBA broadeneds the DSC glass transition and is consistent with a reduction in the DMA tanδ data relaxation intensity (Figure 9b). This could be due in part to intersegmental mixing of hard and soft segments, and/or a restricted chain mobility imposed by the presence of a bidentate hydrogen bonded complex. The latter is similar to the broadening in glass transition observed in chemically cross-linked polyurethanes.[50] Table 4 lists the values of T_g obtained from DSC and DMA measurements, as well as ambient storage modulus data from DMA.

PDA37BBA37 displays a 45.2 ºC increase in its dynamic (DMA) determined T_g to 49.3 ºC relative to the static DSC value (4.1 ºC). The value of dynamic T_g is likely the result of an expanded glass state and transient behavior from rubbery to glassy with dynamic measurements, which is also observed in PDA50BBA50 and PDA60BBA60. The static T_g of PDA60BBA60 is close to ambient temperature, and dynamic T_g behavior is expected. The values of dynamic storage modulus measured at 25 ºC display approximately three-order of magnitude increase from 3.2 MPa

of PDA0BBA0 (a pseudo soft phase) to 1030.8 MPa for PDA60BBA60. Similar observations are noteworthy for PDA0BBA100 (1238.4 MPa) as detailed in Table 2.

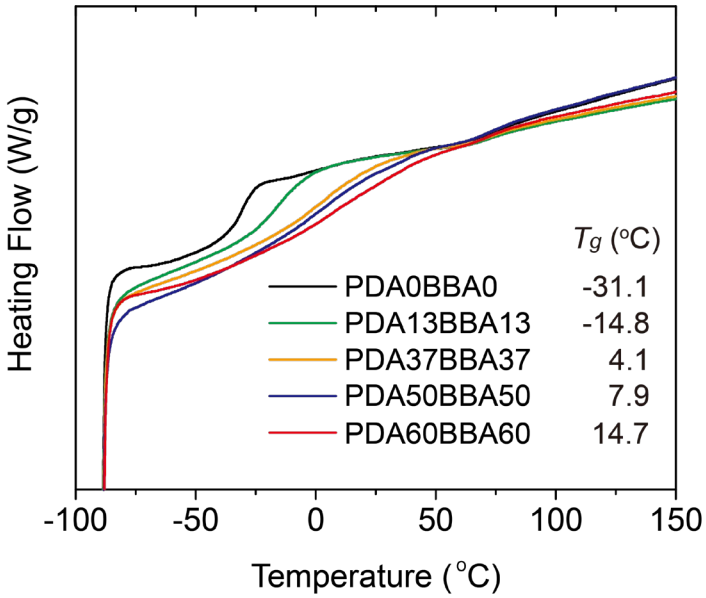

Figure 8. DSC thermograms of PDA0BBA0 (black), PDA13BBA13 (green), PDA37BBA37 (orange), PDA50BBA50 (blue), and PDA60BBA60 (red).

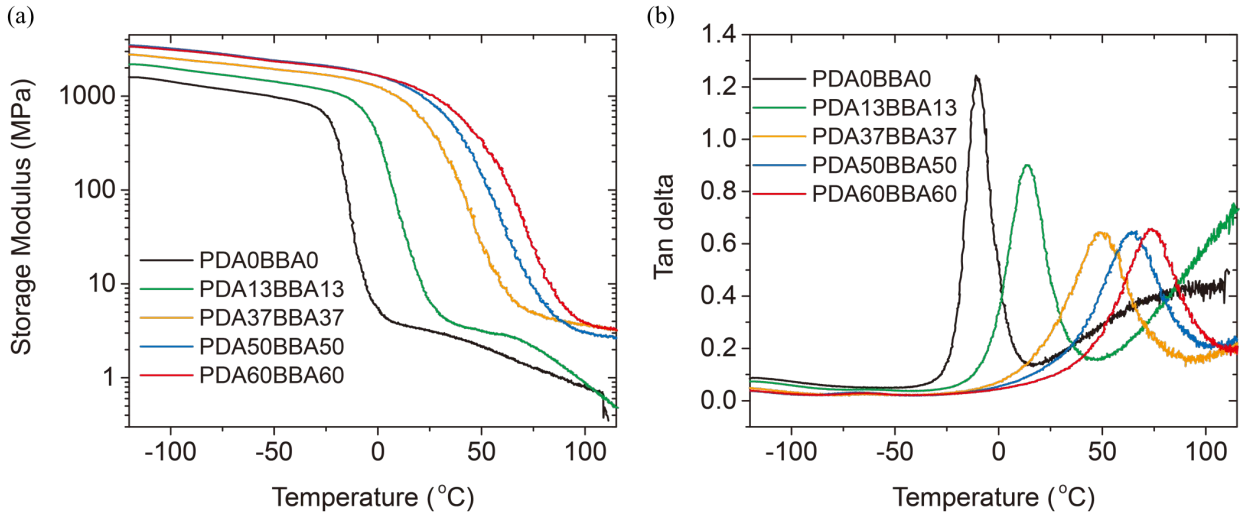

Figure 9. Temperature-dependence of (a) storage modulus and (b) tanδ data obtained at 1 Hz via DMA for PDA0BBA0 (black), PDA13BBA13 (green), PDA37BBA37 (orange), PDA50BBA50 (blue), and PDA60BBA60 (red).

Table 4. Values of T_g determined from DSC and DMA at 1 Hz, as well as values of ambient storage modulus data from DMA for the baseline PDA0BBA0 and PDA/BBA-polyurethanes, as well as for MDI-BDO-650.

	MDI:PDA: BBA:PTMO[a]	M_n (kDa)[b]	PDI	T_g^{DSC} (°C)	T_g^{DMA} (°C)	Storage modulus[c] (MPa)
PDA0BBA0	100:0:0:100	56.5	2.02	-31.1	-11.0	3.2
PDA13BBA13	126:13:13:100	59.0	1.83	-14.8	13.8	6.3
PDA37BBA37	174:37:37:100	37.1	2.27	4.1	49.3	456.3
PDA50BBA50	200:50:50:100	50.8	1.72	7.9	64.4	877.3
PDA60BBA60	220:60:60:100	48.6	1.99	14.7	74.2	1030.8
MDI-BDO-650[d]	-	-	-	-17.2[e]	-2.1[e]	54.3

[a] Molar ratio. [b] THF GPC. [c] Storage modulus at 25 °C. [d] MDI:BDO:PTMO = 200:100:100. [e] The values are consistent with those reported previously.[37]

With an increase in the PDA/BBA content, PDA37BBA37 exhibits significantly greater extent of strain hardening in comparison with PDA13BBA13 and the baseline PDA0BBA0. Both PDA50BBA50 and PDA60BBA60 also reveal a significant increase in modulus, as well as higher flow stress values and strain hardening (Figure 10). Both PDA60BBA60 and PDA50BBA50 have characteristic high stiffness followed by a yield-like event. Specifically, PDA60BBA60 exhibits a higher yield stress along with significantly higher post-yield flow stress values, whereas PDA37BBA37 and PDA50BBA50 have higher tensile strength values and toughness. Consistently PDA60BBA60 has the highest calorimetric T_g value of the PDA/BBA-containing polyurethanes. It is noteworthy that PDA37BBA37 having similar wt.% hard segment content as that of MDI-BDO-650, 50.5% vs. 48.1%, respectively, exhibits significantly greater extent of strain hardening (Table 2), along with higher tensile strength, 65.5 MPa vs. 13.8 MPa, respectively. These observations suggest the efficacy of PDA/BBA to work in concert together, despite PDA37BBA37 having a relatively lower molar content of carbamates than MDI-BDO-650. Table 5 lists the values of flow stress measured at 50% and 200% strain for the baseline PDA0BBA0 and other PDA/BBA-polyurethanes, the tensile strength, strain at failure, along with the calculated toughness for

PDA37BBA37, PDA50BBA50, and PDA60BBA60, as well as the yield stress measured for PDA50BBA50 and PDA60BBA60.

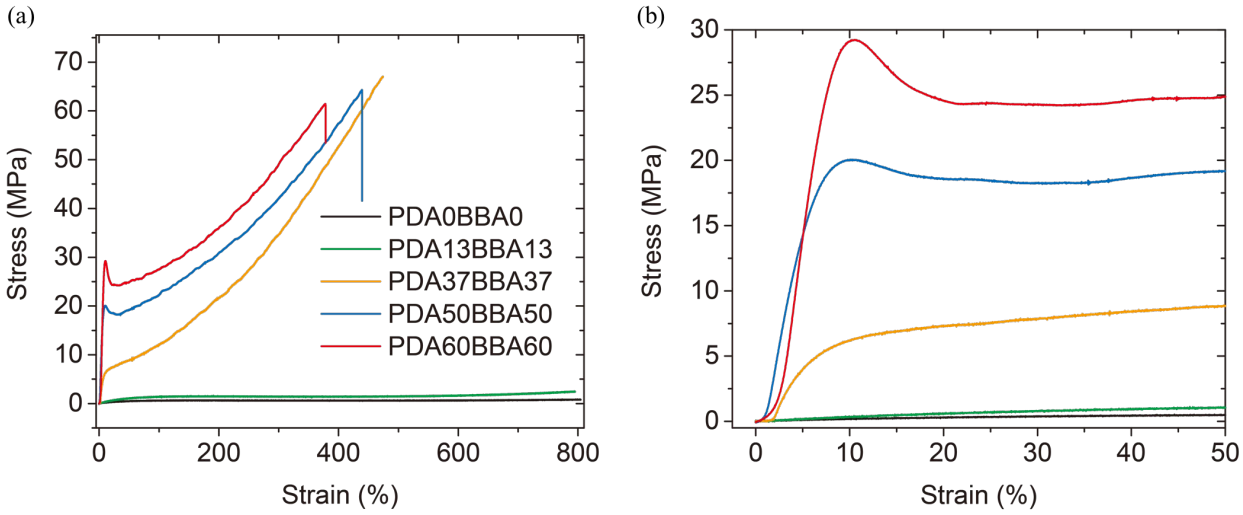

Figure 10. Representative stress-strain data obtained from tensile deformation measurements (a) for PDA0BBA0 (black), PDA13BBA13 (green), PDA37BBA37 (orange), PDA50BBA50 (blue), and PDA60BBA60 (red), and (b) for better visual differentiation of initial stiffness data among PDA37BBA37 (orange), PDA50BBA50 (blue), and PDA60BBA60 (red).

Table 5. Values of flow stress measured at 50% strain and 200% strain, tensile strength, strain at failure, yield stress, and the calculated toughness for PDA/BBA-polyurethanes and MDI-BDO-650.

	Flow stress (MPa)[a]		Tensile Strength (MPa)[a]	Strain at Failure (%)[a]	Yield Stress (MPa)[a]	Tensile Toughness (MJ/m^3)[a]
	at 50% strain	at 200% strain				
PDA0BBA0	0.49[b]	0.63[b]	-	-	-	-
PDA13BBA13	1.04±0.05	1.44±0.02	-	-	-	-
PDA37BBA37	8.94±0.09	21.06±0.80	65.50±6.71	487±42	-	142±21
PDA50BBA50	18.79±0.35	30.64±0.21	67.45±4.13	432±16	19.26±0.66	152±11
PDA60BBA60	25.07±0.35	36.06±0.66	55.82±5.93	343±35	29.61±0.35	122±20

MDI-BDO-650	5.24±0.12	7.53±0.19	13.80±0.46	635±20	-	59±1

[a] Tensile properties were calculated based on the average of three measurements ± standard deviation. [b] An average of two measurements.

4. Discussion

To best illustrate the synergy associated with PDA/BBA in polyurethanes, we compare the flow stress values measured at deformations of 50% strain and 200% strain, respectively, as a function of hard segment content. As shown in Figure 11, the extent of strain hardening becomes more significant as the PDA/BBA hard segment content increases in PDA37BBA37, PDA50BBA50, and PDA60BBA60. PDA50BBA50 and PDA60BBA60 exhibit a yielding deformation behavior like PDA0BBA100 under quasistatic tensile loading (Figure 12), where PDA60BBA60 reveals a higher yield stress determined at 29.6 MPa than PDA0BBA100 (23.9 MPa). The mechanical strengthening in PDA60BBA60 could be a result of significant intersegmental mixing and/or a supramolecular PDA/BBA complex. The latter requires PDA to be above a percolation threshold concentration to produce an interconnected network. It is noteworthy that addition of PDA and BBA gives rise to a glass-like hierarchical structure in both PDA50BBA50 and PDA60BBA60 with greatly enhanced thermal and mechanical properties (Tables 4 and 5, respectively), yet they are not chemically crosslinked.

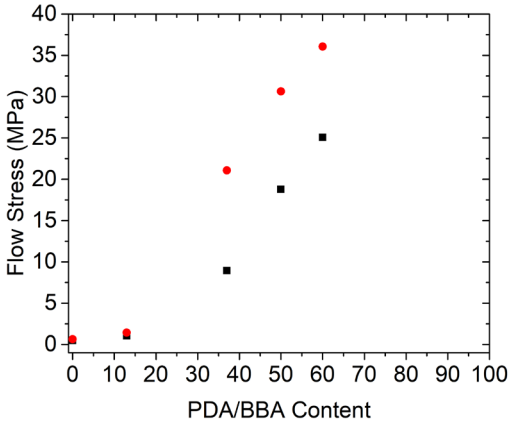

Figure 11. Comparison of flow stress determined at 50% strain (black) and 200% strain (red) as a function of PDA/BBA hard segment content in PDA/BBA-polyurethanes.

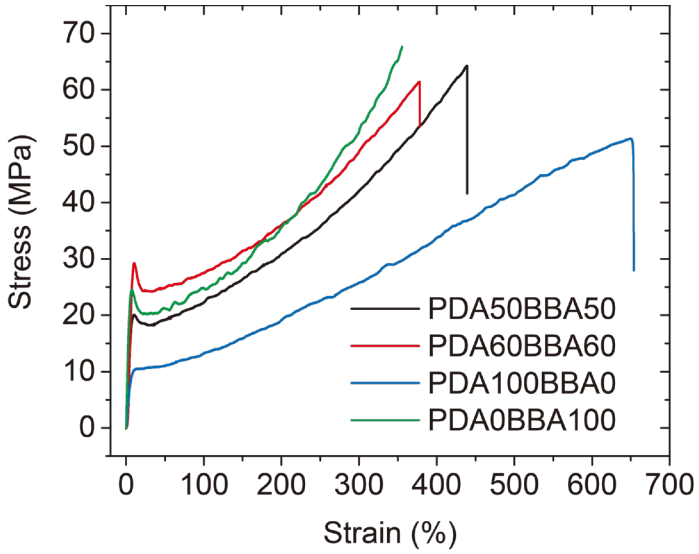

Figure 12. Comparison of tensile stress-strain data for PDA50BBA50 (black), PDA60BBA60 (red), PDA100BBA0 (blue), and PDA0BBA100 (green).

To further elucidate the significance of the dynamic T_g*s*, we compare the shift of T_g from calorimetric measurements to those determined at 1Hz via DMA among the PDABBA-containing polyurethanes and MDI-BDO-650. This variation is illustrated in Figure 13 in terms of log(frequency) vs. reciprocal temperature, where the enthalpy relaxation time for calorimetric T_g measurements is assigned as 100 s,[22] which corresponds to an equivalent frequency of 0.0016 Hz. Increased PDA/BBA content in PDA60BBA60, PDA50BBA50, and PDA37BBA37 produced a greater frequency-dependency than PDA13BBA13, baseline PDA0BBA0 without any hard segment, and MDI-BDO-650. PDA produces greater changes in dynamic T_g than BBA, and PDA100BBA0 displays a 60.6ºC increase (from 7 ºC to 67.6 ºC) vs. 46.9 ºC (from 14.6 ºC to 61.5 ºC) for PDA0BBA100 (Table 2). In comparison, PDA50BBA50 and PDA60BBA60 exhibit comparable T_g values and frequency-dependency as PDA100BBA0 and PDA0BBA100, as shown in Figure 16. Again, the differences in static and dynamic T_g strongly suggest an interplay between intersegmental mixing and supramolecular hydrogen bond interactions in PDA/BBA-polyurethanes. These observations affirm new designs of robust hierarchical polyurethanes not only for optimization of both calorimetric T_g and dynamic T_g, but also with capability to facilitate a transient dynamic stiffening response. In the future work, we will perform high strain-rate microparticle impact measurements through a laser induced particle impact test platform to further

validation of dynamic stiffening and strengthening characteristics, along with the use of ^{13}C ssNMR dipolar dephasing characterization to better discern and differentiate the influence of PDA and BBA on the segmental dynamics associated with PTMO.

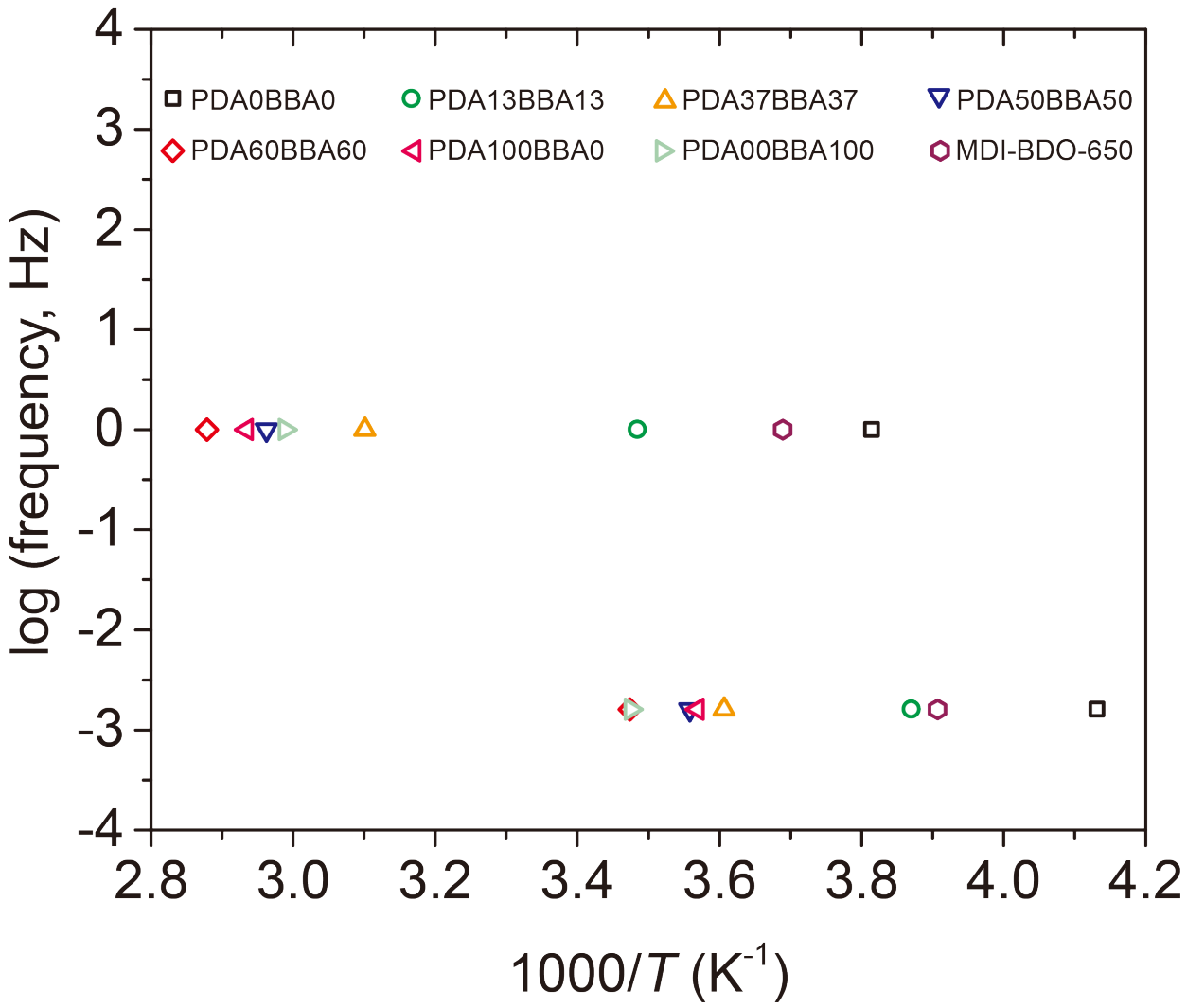

Figure 13. Comparison of the shift of T_g obtained from DMA (1 Hz) and calorimetric T_g from DSC (equivalent to 0.0016 Hz) for PDA0BBA0 (black square), PDA13BBA13 (green circle), PDA37BBA37 (orange up triangle), PDA50BBA50 (blue down triangle), PDA60BBA60 (red diamond), PDA100BBA0 (pink left triangle), PDA0BBA100 (light green right triangle), and MDI-BDO-650 (purple hexagon).

5. Conclusion

We have successfully demonstrated a supramolecular design strategy to create robust hierarchical polyurethane elastomers and its use for thermal and mechanical property optimization. Addition of PDA facilitates the bidentate hydrogen bonding interactions between the carboxamide protons of PDA and carbonyls of carbamates, leading to the formation of a supramolecular complex. PDA100BBA0 exhibits a modest interference peak, but with significantly lower scattering contrast in SAXS than that of the microphase-separated MDI-BDO-650 analog. In comparison, BBA affords dual hydrogen bonding interactions with carbamates in the soft phase and correspondingly greater intersegmental mixing, as evidenced by the presence of significantly lower scattering contrast in SAXS, and a high T_g in PDA0BBA100. In PDA/BBA-based polyurethane elastomers, PDA and BBA are complementary. Higher cohesive energy densities from intersegmental mixing and supramolecular hydrogen bond interactions represent a plausible molecular pathway toward greater strain hardening and strengthening characteristics observed under quasistatic tensile deformation measurements. Additionally, it is envisioned that the presence of multiple intermolecular hydrogen bond interactions in PDA/BBA polyurethanes can be used to create hierarchical elastomers with self-healing capability and the ability to affect T_g suggests potential utility to produce shape memory functionality.

It is noteworthy that PDA37BBA37, PDA50BBA50 and PDA60BBA60 significantly outperform the microphase-separated MDI-BDO-650 analog. The efficacy of PDA/BBA to work in concert together is further elucidated in PDA37BBA37, which has a similar wt.% hard segment content, but a relatively lower carbamate molar content than MDI-BDO-650. PDA37BBA37 exhibits greater extent of strain hardening along with higher tensile strength and tensile toughness values than MDI-BDO-650. Increased PDA/BBA content gives rise to a glass-like hierarchical structure in both PDA50BBA50 and PDA60BBA60, and additionally results in a significant increase of the dynamic T_g, by ~60 °C, which is in contrast to the 15 °C increase observed in the MDI-BDO-PTMO analog. These new insights suggest supramolecular approaches are viable for design of robust hierarchical elastomers for dynamic stiffening and strengthening characteristics optimization which are greatly desired for protection applications.

ACKNOWLEDGMENTS

This manuscript is based upon work supported by the U.S. Army Combat Capabilities Development Command, Army Research Office and Army Research Laboratory, through the Institute for Soldier Nanotechnologies, under Cooperative Agreement Number W911NF-18-2-0048. We thank Keith Husted for his assistant in preparing the dog-bone specimens for tensile measurements.

ABBREVIATIONS

PDA, N^2,N^6-bis(2-hydroxyethyl)pyridine-2,6-dicarboxamide; BBA, 5,5-bis(3-hydroxypropyl)barbituric acid; MDI, 4,4′-methylenediphenyl diisocyanate; PTMO, poly(tetramethylene oxide); DMA, dynamic mechanical analysis; DSC, differential scanning calorimetry; SAXS, small-angle X-ray scattering.

REFERENCES

[1] C.B. Wang, S.L. Cooper, Morphology and properties of segmented polyether polyurethaneureas, Macromolecules 16(5) (1983) 775-786. https://doi.org/10.1021/ma00239a014.

[2] S. Abouzahr, G.L. Wilkes, Z. Ophir, Structure-property behaviour of segmented polyether-MDI-butanediol based urethanes: effect of composition ratio, Polymer 23(7) (1982) 1077-1086. https://doi.org/10.1016/0032-3861(82)90411-6.

[3] J.T. Koberstein, A.F. Galambos, L.M. Leung, Compression-molded polyurethane block copolymers. 1. Microdomain morphology and thermomechanical properties, Macromolecules 25(23) (1992) 6195-6204. https://doi.org/10.1021/ma00049a017.

[4] M. Furukawa, Y. Hamada, K. Kojio, Aggregation structure and mechanical properties of functionally graded polyurethane elastomers, J. Polym. Sci. B Polym. Phys. 41(20) (2003) 2355-2364. https://doi.org/10.1002/polb.10628.

[5] J.P. Sheth, A. Aneja, G.L. Wilkes, E. Yilgor, G.E. Atilla, I. Yilgor, F.L. Beyer, Influence of system variables on the morphological and dynamic mechanical behavior of polydimethylsiloxane based segmented polyurethane and polyurea copolymers: a comparative perspective, Polymer 45(20) (2004) 6919-6932. https://doi.org/10.1016/j.polymer.2004.06.057.

[6] R.A. Koevoets, R.M. Versteegen, H. Kooijman, A.L. Spek, R.P. Sijbesma, E.W. Meijer, Molecular Recognition in a Thermoplastic Elastomer, J. Am. Chem. Soc. 127(9) (2005) 2999-3003. https://doi.org/10.1021/ja0451160.

[7] L.T.J. Korley, B.D. Pate, E.L. Thomas, P.T. Hammond, Effect of the degree of soft and hard segment ordering on the morphology and mechanical behavior of semicrystalline segmented polyurethanes, Polymer 47(9) (2006) 3073-3082. https://doi.org/10.1016/j.polymer.2006.02.093.
[8] K. Kojio, S. Nakashima, M. Furukawa, Microphase-separated structure and mechanical properties of norbornane diisocyanate-based polyurethanes, Polymer 48(4) (2007) 997-1004. https://doi.org/10.1016/j.polymer.2006.12.057.
[9] S. Das, D.F. Cox, G.L. Wilkes, D.B. Klinedinst, I. Yilgor, E. Yilgor, F.L. Beyer, Effect of Symmetry and H-bond Strength of Hard Segments on the Structure-Property Relationships of Segmented, Nonchain Extended Polyurethanes and Polyureas, J. Macromol. Sci., Part B 46(5) (2007) 853-875. https://doi.org/10.1080/00222340701388805.
[10] M.A. Hood, B. Wang, J.M. Sands, J.J. La Scala, F.L. Beyer, C.Y. Li, Morphology control of segmented polyurethanes by crystallization of hard and soft segments, Polymer 51(10) (2010) 2191-2198. https://doi.org/10.1016/j.polymer.2010.03.027.
[11] I. Yilgör, E. Yilgör, G.L. Wilkes, Critical parameters in designing segmented polyurethanes and their effect on morphology and properties: A comprehensive review, Polymer 58 (2015) A1-A36. https://doi.org/10.1016/j.polymer.2014.12.014.
[12] Lubrizol. https://www.lubrizol.com/Engineered-Polymers/Products/Estane-TPU (accessed 2022-05-01).
[13] M. Sáenz-Pérez, T. Bashir, J.M. Laza, J. García-Barrasa, J.L. Vilas, M. Skrifvars, L.M. León, Novel shape-memory polyurethane fibers for textile applications, Text. Res. J. 89(6) (2018) 1027-1037. https://doi.org/10.1177/0040517518760756.
[14] Wikipedia. https://en.wikipedia.org/wiki/Polyurethane (accessed 2022-05-01).
[15] R.J. Zdrahala, I.J. Zdrahala, Biomedical Applications of Polyurethanes: A Review of Past Promises, Present Realities, and a Vibrant Future, J. Biomater. Appl. 14(1) (1999) 67-90. https://doi.org/10.1177/088532829901400104.
[16] J. Joseph, R.M. Patel, A. Wenham, J.R. Smith, Biomedical applications of polyurethane materials and coatings, Trans. IMF 96(3) (2018) 121-129. https://doi.org/10.1080/00202967.2018.1450209.
[17] S. Wendels, L. Avérous, Biobased polyurethanes for biomedical applications, Bioact. Mater. 6(4) (2021) 1083-1106. https://doi.org/10.1016/j.bioactmat.2020.10.002.

[18] K. Karthikeyan, B.P. Russell, N.A. Fleck, H.N.G. Wadley, V.S. Deshpande, The effect of shear strength on the ballistic response of laminated composite plates, Eur. J. Mech. A/Solids 42 (2013) 35-53. https://doi.org/10.1016/j.euromechsol.2013.04.002.

[19] R.B. Bogoslovov, C.M. Roland, R.M. Gamache, Impact-induced glass transition in elastomeric coatings, Appl. Phys. Lett. 90(22) (2007) 221910. https://doi.org/10.1063/1.2745212.

[20] C.M. Roland, D. Fragiadakis, R.M. Gamache, Elastomer–steel laminate armor, Compos. Struct. 92(5) (2010) 1059-1064. https://doi.org/10.1016/j.compstruct.2009.09.057.

[21] C.M. Roland, R. Casalini, Effect of hydrostatic pressure on the viscoelastic response of polyurea, Polymer 48(19) (2007) 5747-5752. https://doi.org/10.1016/j.polymer.2007.07.017.

[22] D. Fragiadakis, R. Gamache, R.B. Bogoslovov, C.M. Roland, Segmental dynamics of polyurea: Effect of stoichiometry, Polymer 51(1) (2010) 178-184. https://doi.org/10.1016/j.polymer.2009.11.028.

[23] T. Choi, D. Fragiadakis, C.M. Roland, J. Runt, Microstructure and Segmental Dynamics of Polyurea under Uniaxial Deformation, Macromolecules 45(8) (2012) 3581-3589. https://doi.org/10.1021/ma300128d.

[24] A.M. Castagna, A. Pangon, T. Choi, G.P. Dillon, J. Runt, The Role of Soft Segment Molecular Weight on Microphase Separation and Dynamics of Bulk Polymerized Polyureas, Macromolecules 45(20) (2012) 8438-8444. https://doi.org/10.1021/ma3016568.

[25] S.S. Sarva, A.J. Hsieh, The effect of microstructure on the rate-dependent stress–strain behavior of poly(urethane urea) elastomers, Polymer 50(13) (2009) 3007-3015. https://doi.org/10.1016/j.polymer.2009.04.025.

[26] R.G. Rinaldi, A.J. Hsieh, M.C. Boyce, Tunable microstructures and mechanical deformation in transparent poly(urethane urea)s, J. Polym. Sci., Part B: Polym. Phys. 49(2) (2011) 123-135. https://doi.org/10.1002/polb.22128.

[27] K.E. Strawhecker, A.J. Hsieh, T.L. Chantawansri, Z.I. Kalcioglu, K.J. Van Vliet, Influence of microstructure on micro-/nano-mechanical measurements of select model transparent poly(urethane urea) elastomers, Polymer 54(2) (2013) 901-908. https://doi.org/10.1016/j.polymer.2012.12.018.

[28] T.L. Chantawansri, Y.R. Sliozberg, J.W. Andzelm, A.J. Hsieh, Coarse-grained modeling of model poly(urethane urea)s: Microstructure and interface aspects, Polymer 53(20) (2012) 4512-4524. https://doi.org/10.1016/j.polymer.2012.07.056.

[29] W. Hu, A.J. Hsieh, Phase-mixing and molecular dynamics in poly(urethane urea) elastomers by solid-state NMR, Polymer 54(22) (2013) 6218-6225. https://doi.org/10.1016/j.polymer.2013.09.010.

[30] A.J. Hsieh, T.L. Chantawansri, W. Hu, K.E. Strawhecker, D.T. Casem, J.K. Eliason, K.A. Nelson, E.M. Parsons, New insight into microstructure-mediated segmental dynamics in select model poly(urethane urea) elastomers, Polymer 55(7) (2014) 1883-1892. https://doi.org/10.1016/j.polymer.2014.02.037.

[31] D. Veysset, A.J. Hsieh, S. Kooi, A.A. Maznev, K.A. Masser, K.A. Nelson, Dynamics of supersonic microparticle impact on elastomers revealed by real–time multi–frame imaging, Sci. Rep. 6(1) (2016) 25577. https://doi.org/10.1038/srep25577.

[32] D. Veysset, A.J. Hsieh, S.E. Kooi, K.A. Nelson, Molecular influence in high-strain-rate microparticle impact response of poly(urethane urea) elastomers, Polymer 123 (2017) 30-38. https://doi.org/10.1016/j.polymer.2017.06.071.

[33] A.J. Hsieh, D. Veysset, D.F. Miranda, S.E. Kooi, J. Runt, K.A. Nelson, Molecular influence in the glass/polymer interface design: The role of segmental dynamics, Polymer 146 (2018) 222-229. https://doi.org/10.1016/j.polymer.2018.05.034.

[34] A.M. Castagna, D. Fragiadakis, H. Lee, T. Choi, J. Runt, The Role of Hard Segment Content on the Molecular Dynamics of Poly(tetramethylene oxide)-Based Polyurethane Copolymers, Macromolecules 44(19) (2011) 7831-7836. https://doi.org/10.1021/ma2017138.

[35] D. Fragiadakis, J. Runt, Molecular Dynamics of Segmented Polyurethane Copolymers: Influence of Soft Segment Composition, Macromolecules 46(10) (2013) 4184-4190. https://doi.org/10.1021/ma4006395.

[36] Y.-C.M. Wu, W. Hu, Y. Sun, D. Veysset, S.E. Kooi, K.A. Nelson, T.M. Swager, A.J. Hsieh, Unraveling the high strain-rate dynamic stiffening in select model polyurethanes − the role of intermolecular hydrogen bonding, Polymer 168 (2019) 218-227. https://doi.org/10.1016/j.polymer.2019.02.038.

[37] Y. Sun, Y.-C.M. Wu, D. Veysset, S.E. Kooi, W. Hu, T.M. Swager, K.A. Nelson, A.J. Hsieh, Molecular dependencies of dynamic stiffening and strengthening through high strain rate microparticle impact of polyurethane and polyurea elastomers, Appl. Phys. Lett. 115(9) (2019) 093701. https://doi.org/10.1063/1.5111964.

[38] A.J. Hsieh, Y.-C. Mason Wu, W. Hu, J.P. Mikhail, D. Veysset, S.E. Kooi, K.A. Nelson, G.C. Rutledge, T.M. Swager, Bottom-up design toward dynamically robust polyurethane elastomers, Polymer 218 (2021) 123518. https://doi.org/10.1016/j.polymer.2021.123518.

[39] A.M. Nelson, T.E. Long, Synthesis, Properties, and Applications of Ion-Containing Polyurethane Segmented Copolymers, Macromol. Chem. Phys. 215(22) (2014) 2161-2174. https://doi.org/10.1002/macp.201400373.

[40] R.H. Lambeth, M.H. Baranoski, A.M. Savage, B.F. Morgan, F.L. Beyer, B.A. Mantooth, N.E. Zander, Synthesis and Characterization of Segmented Polyurethanes Containing Trisaminocyclopropenium Carbocations, ACS Macro Lett. 7(7) (2018) 846-851. https://doi.org/10.1021/acsmacrolett.8b00395.

[41] R.-h. Song, Z.-h. Liu, X. Geng, L. Ye, A.-y. Zhang, Z.-g. Feng, Preparation and characterization of cross-linked polyurethanes using β-CD [3]PR as slide-ring cross-linker, Polymer 249 (2022) 124862. https://doi.org/10.1016/j.polymer.2022.124862.

[42] C.W. Carpenter, M.G. Malinao, T.A. Rafeedi, D. Rodriquez, S.T.M. Tan, N.B. Root, K. Skelil, J. Ramírez, B. Polat, S.E. Root, V.S. Ramachandran, D.J. Lipomi, Electropneumotactile Stimulation: Multimodal Haptic Actuators Enabled by a Stretchable Conductive Polymer on Inflatable Pockets, Adv. Mater. Technol. 5(6) (2020) 1901119. https://doi.org/10.1002/admt.201901119.

[43] F. Sugiyama, A.T. Kleinschmidt, L.V. Kayser, M.A. Alkhadra, J.M.H. Wan, A.S.C. Chiang, D. Rodriquez, S.E. Root, S. Savagatrup, D.J. Lipomi, Stretchable and Degradable Semiconducting Block Copolymers, Macromolecules 51(15) (2018) 5944-5949. https://doi.org/10.1021/acs.macromol.8b00846.

[44] S.-R. Mo, J.-C. Lai, K.-Y. Zeng, D.-P. Wang, C.-H. Li, J.-L. Zuo, New insights into the mechanical and self-healing properties of polymers cross-linked by Fe(III)-2,6-pyridinedicarboxamide coordination complexes, Poly. Chem. 10(3) (2019) 362-371. https://doi.org/10.1039/C8PY01233D.

[45] M. Zulkefeli, Y. Hisamatsu, A. Suzuki, Y. Miyazawa, M. Shiro, S. Aoki, Supramolecular Phosphatases Formed by the Self-Assembly of the Bis(Zn^{2+}–Cyclen) Complex, Copper(II), and Barbital Derivatives in Water, Chem. Asian J. 9(10) (2014) 2831-2841. https://doi.org/10.1002/asia.201402513.

[46] M.A. Ayer, Y.C. Simon, C. Weder, Azo-Containing Polymers with Degradation On-Demand Feature, Macromolecules 49(8) (2016) 2917-2927. https://doi.org/10.1021/acs.macromol.6b00418.

[47] Y. Sagara, M. Karman, E. Verde-Sesto, K. Matsuo, Y. Kim, N. Tamaoki, C. Weder, Rotaxanes as Mechanochromic Fluorescent Force Transducers in Polymers, J. Am. Chem. Soc. 140(5) (2018) 1584-1587. https://doi.org/10.1021/jacs.7b12405.

[48] K. Husted, A. Herzog-Arbeitman, D. Kleinschmidt, W. Zhang, A. Fielitz, A. Le, M. Zhong, J. Johnson, Diversity-Oriented Synthesis of Graft Copolymer Silicones Enables Exceptionally Broad Thermomechanical Property Windows through Pendant-Mediation, Preprint available at Research Square (2022) doi:10.21203/rs.3.rs-1115203/v1.

[49] T.J. Bartczak, Z.M. Michalska, B. Ostaszewski, P. Sobota, K. Strzelec, Synthesis, characterization and X-ray structures of the model ligand for a coordination polymer: diethyl-2,6-pyridine dicarboxamide and its complex with $PdCl_2$, Inorg. Chim. Acta 319(1) (2001) 229-234. https://doi.org/10.1016/S0020-1693(01)00455-8.

[50] S. Oprea, V.-O. Potolinca, V. Oprea, Synthesis and properties of new crosslinked polyurethane elastomers based on isosorbide, Eur. Polym. J. 83 (2016) 161-172. https://doi.org/10.1016/j.eurpolymj.2016.08.020.